Coherent control of laser-induced breakdown

M. Y. Shverdin, S. N. Goda, G. Y. Yin, and S. E. Harris

Edward L. Ginzton Laboratory, Stanford University, Stanford, California 94305

Received November 11, 2005; accepted January 3, 2006; posted January 30, 2006 (Doc. ID 65951)

We demonstrate coherent control of laser-induced optical breakdown in Ar and Xe with a femtosecond time-scale pulse train. By using a genetic algorithm to set the relative phases of seven optical sidebands that span two octaves of bandwidth, we enhance or suppress the probability of breakdown, vary the onset time of the spark, and to some extent, vary the position of the spark and the timing of the laser-produced shock wave.

OCIS codes: 140.3440, 190.7110, 320.2250, 320.7110.

Recently we have described a light source that has seven spectral components that span the spectral region of 1.56 μm–410 nm.[1] By using a liquid-crystal spatial light modulator, we have demonstrated the synthesis of controllable optical waveforms, and, in particular, a train of single-cycle optical pulses. This train of pulses occurs beneath a Q-switched, 10 ns envelope with a total energy of approximately 10 mJ and a repetition rate of 10 Hz. The individual single-cycle pulses have a pulse width of 1.6 fs, a pulse separation of 11 fs, and a peak power of 1 MW. This Letter describes experiments in which we use a genetic algorithm (GA) to adjust the phases of these seven spectral components to control certain properties of laser-induced breakdown in a target gas.

When a sufficiently intense laser beam interacts with a medium, gas breakdown occurs through the interplay of multiphoton ionization and inverse bremsstrahlung-driven avalanching.[2] Multiphoton ionization is dependent on the temporal waveform, which is controlled by adjusting the phases of the incident beam. Conversely, inverse bremsstrahlung and avalanching depend only on average power density (approximately 3 GW/cm^2). These processes interplay because the temporal waveform determines how early (under the Q-switched envelope) a typical electron is ionized and begins to gain energy from the optical field. As will be seen below, the probability of breakdown, the timing of the spark, and the arrival time of the laser-induced shock wave may each be controlled.

The control of laser-induced breakdown has been studied extensively and is important for materials processing, spark ignition, and laser switching.[3–5] Recently, in the spirit of this work, terawatt-scale pulses of 100 fs in duration have been shown to trigger white-light filamentation in the atmosphere, and dispersion compensation has been used to vary the location of filamentation.[6] More generally, experiments using evolutionary algorithms to shape femtosecond pulses have varied the branching ratio of molecular dissociation,[7] excited different Raman modes in a molecule,[8] and shaped high-order harmonic spectra.[9]

To obtain a spectrum of approximately two octaves in width we use two intense, Q-switched lasers slightly detuned from the Raman resonance to adiabatically excite the fundamental vibrational transition in D_2 (Fig. 1). A discrete spectrum of frequency components equally spaced by 2994 cm^{-1} and spanning almost four octaves is generated. A seven-sideband subset is dispersed and passed through a Jenoptik liquid-crystal spatial light modulator. The beams are recombined and focused into a 15 cm long gas chamber by using a 15 cm achromatic lens. The phases of these sidebands are independently adjusted so as to synthesize a controllable waveform in the target chamber.[1,10]

A CCD camera monitors the focal region of the incident beams in the gas cell. A 75 mm lens images the focal region onto a Si photodiode (PD). When breakdown occurs we observe a white, nearly circular spark $\approx$2 mm long. This spark is detected by the CCD and the PD. The PD signal goes to a Stanford Research Systems boxcar integrator that outputs to a computer through a data acquisition board (NI PCI-1200). The image on the CCD is used to align the PD. In each of the experiments described below, we use a GA[11] to adjust the phases of the sidebands and to evolve to the optimum pulse shape that maximizes or minimizes a selected property (the fitness function).

Because of the ±10% variation in pulse-to-pulse energy, only a fraction of the incident Q-switched pulses result in breakdown. We optimize a fitness function that is the fraction of 50 incident pulses that causes breakdown. Breakdown is said to occur when the integrated PD signal exceeds a set threshold. The GA utilizes 10 pulse shapes per generation and executes 7–10 generations to converge to the optimal set of 7

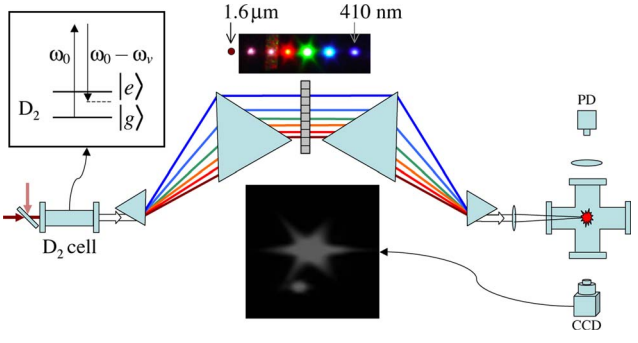

Fig. 1. (Color online) Experimental setup: Seven Raman sidebands are generated in the D_2 cell, dispersed, passed through a spatial light modulator, and recombined in the gas chamber. The breakdown spark is imaged by the CCD.

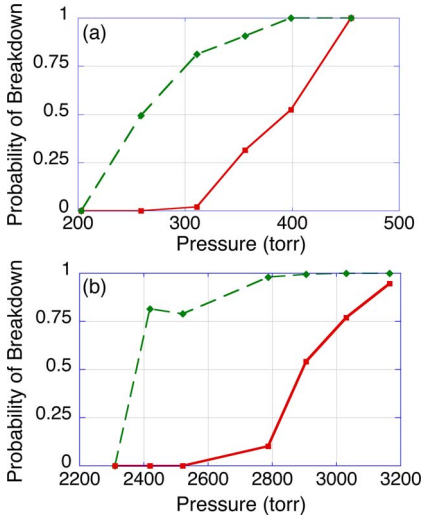

Fig. 2. (Color online) Control of the probability of gas breakdown. The fraction of 400 consecutive Q-switched laser pulses that produce gas breakdown is plotted versus the pressure of (a) Xe and (b) argon gas. The relative Raman sideband phases are determined by the GA to either maximize (circles) or minimize (squares) the probability of breakdown. The incident energies at 1.56 μm, 1.064 μm, 807 nm, 650 nm, 544 nm, 468 nm, and 410 nm are, respectively, 1.0, 2.5, 0.8, 1.9, 1.1, 0.7, and 0.4 mJ.

phases. Each optimization at a named pressure requires $\approx$15 min due to the 10 Hz lasers.

The ability to control the probability of gas breakdown is demonstrated in Fig. 2. Each point represents the probability of breakdown as averaged over 400 laser shots. The dashed curve connects the points for breakdown maximization, and the solid curve connects the points for breakdown minimization. The probability may be set to a value within the two curves. In Xe [Fig. 2(a)] the incident pulse shape effects the probability of breakdown in the pressure range from 200 to 450 Torr, whereas in Ar [Fig. 2(b)] the region of control occurs in the pressure range from 2300 to 3200 Torr. At pressures below the lower bounds, breakdown never occurs; above the upper bounds, breakdown always occurs.

We find that the sensitivity to phase variation increases as the confocal parameter in the target cell is reduced. In Fig. 2 an $f=15$ cm achromat was used. With an $f=20$ cm achromat, only a small amount of control was observed; with an $f=25$ cm or longer achromat, no control over the probability of breakdown was observable. This is consistent with a picture in which the GA attempts to form a particular pulse shape that is preserved over a length that is limited by the dispersion in the gas.

Next we apply the GA to vary the onset time of the laser-induced spark (recombination radiation) in Xe at 390 Torr. The spark forms 3–7 ns following the peak of the Q-switched pulse (Fig. 3) and grows brighter as the plasma absorbs laser radiation for the duration of the pulse. The recombination radiation remains visible for over 200 ns ($1/e^2$ of peak intensity). Here the optimizable parameter (the fitness function) is defined as the PD signal integrated over the gated time interval (the $\approx$8 ns wide shaded rectangle in Fig. 3). To attain the maximum or minimum onset delay, the GA executes 5–7 generations, each consisting of 10 sets of phases.

The minimum onset delay recombination radiation signal is shown by curve (a) in Fig. 3. The plotted curve is a mean of the measured recombination energy versus time data from 100 Q-switched laser shots. The signal representing maximum onset delay is shown by curve (b) in Fig. 3, which is an average from 84 Q-switched laser shots. The probability of breakdown for curve (a) is 100% while that for curve (b) is 84%. Note that the intensity of the recombination radiation is inversely correlated with the onset time.

We next explore the acoustic shock wave generated when the plasma absorbs laser radiation, heats, and expands. The size and intensity of the spark depends on the probability of ionization and the duration of the laser pulse. After the plasma stops growing the shock separates from the plasma and propagates through the cell at sonic velocity.[12] As it propagates, the shock wave modulates the refractive index of the medium.

Working in Xe at 550 Torr we send a 6 mW, 1 mm diameter cw HeNe beam perpendicularly through a region in the chamber $\approx$1 mm away from the plasma [Fig. 4(a)]. A PD located on the opposite side of the

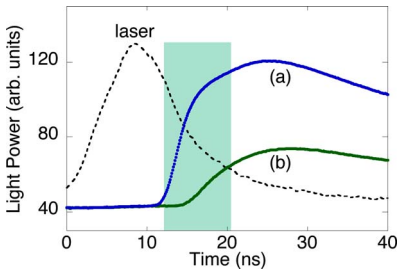

Fig. 3. (Color online) Control of recombination radiation onset. Curves (a) and (b) result from two different sets of relative phases determined by the GA to (a) maximize or (b) minimize the integrated signal during the gated time (shaded rectangle). The onset is varied by 3.4±2.0 ns.

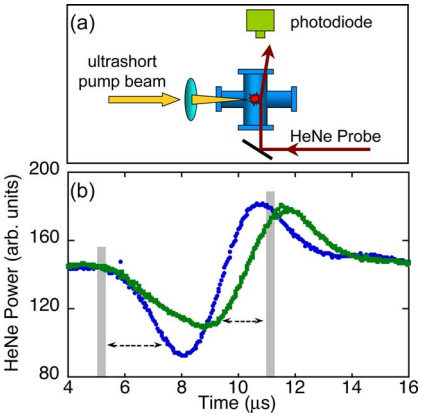

Fig. 4. (Color online) Control of spark location. (a) a HeNe beam propagates through the Xe cell away from the spark and is detected by a photodiode. (b) The detected power variation signifies the shock-wave arrival. The GA determines the relative sideband phases that minimize the HeNe energy within the corresponding time intervals (shaded rectangles).

chamber measures the HeNe beam power. Several microseconds after the plasma is formed, the HeNe signal on the PD decreases and then increases with a total deviation time of 9 μs [Fig. 4(b)]. The dip in the HeNe signal is caused by shock-wave-induced deflection; the increase above the baseline level results from the higher density and focusing of the beam at the trailing end of the shock.

The shock arrival time depends on the distance between the spark and the HeNe beam. We measure the speed of the shock by axially translating the focusing lens and recording the corresponding time of the PD signal minima. The measured speed of 210 ± 20 m/s is within 17% of the theoretical speed of sound in Xe at STP (180 m/s). The shock-wave signature repeats every 60 to 70 μs, roughly corresponding to the reflection off the chamber walls (chamber radius ≈ 1 cm).

Next we use the shock arrival time to determine the mean position of the generated spark and to show that this mean position may be translated by varying the relative phases of the seven Raman sidebands with the GA. The location of the spark dances at the focus, resulting in a standard deviation in arrival time of ≈ 320 ns. The fitness function is the integrated PD signal within a gated time interval and is always minimized. To translate the spark toward the HeNe beam [the dark curve in Fig. 4(b)], the gate is set prior to the shock arrival. To move the spark farther away [the light curve in Fig. 4(b)], the gate is set near the maximum of the PD signal. Each plotted curve is a mean over 34 Q-switched laser shots. The minima are separated by 600 ± 470 ns, implying that on average the spark has translated by 130 ± 97 μm, or 2% of the confocal parameter.

We have attempted to ascertain the temporal pulse shapes that correspond to the GA-optimized phases of the experiments described in this Letter. While we find that the optimum phases are reproducible over separate executions of the GA, imprecise knowledge of the density–length product and also of the refractive indices does not allow us to determine the temporal waveform at the target point.

The authors thank Phil Bucksbaum for his many insights. This work was supported by the U.S. Air Force Office of Scientific Research and the U.S. Army Research Office. M. Y. Shverdin's email address is mshverdin@gmail.com.

Note added in proof: During the preparation of this manuscript, we became aware of a related work in which a GA was used to control the position and extent of white-light filaments in an aqueous solution.[13]

References

1. M. Y. Shverdin, D. R. Walker, D. D. Yavuz, G. Y. Yin, and S. E. Harris, Phys. Rev. Lett. **94**, 033904 (2005).
2. G. M. Weyl and D. Rosen, Phys. Rev. A **31**, 2300 (1985).
3. C. Momma, B. N. Chichkov, S. Nolte, F. Alvensleben, A. Tünnermann, H. Welling, and B. Wellegehausen, Opt. Commun. **129**, 134 (1996).
4. V. Kumar and R. K. Thareja, Appl. Opt. **31**, 3460 (1992).
5. T. X. Phuoc, Opt. Commun. **175**, 419 (2000).
6. J. Kasparian, M. Rodriguez, G. Mejean, J. Yu, E. Salmon, H. Willie, R. Bourayou, S. Frey, Y.-B. Andre, A. Mysyrowicz, R. Sauerbrey, J.-P. Wolf, and L. Woste, Science **301**, 61 (2003).
7. A. Assion, T. Baumert, M. Bergt, T. Brixner, B. Kiefer, V. Seyfried, M. Strehle, and G. Gerber, Science **282**, 919 (1998).
8. B. J. Pearson and P. H. Bucksbaum, Phys. Rev. Lett. **92**, 243 (2004).
9. R. Bartels, S. Backus, E. Zeek, L. Misoguti, G. Vdovin, I. P. Christov, M. M. Murnane, and H. C. Kapteyn, Nature **406**, 164 (2000).
10. D. D. Yavuz, D. R. Walker, M. Y. Shverdin, G. Y. Yin, and S. E. Harris, Phys. Rev. Lett. **91**, 233 (2003).
11. J. J. Grefenstette, "Genesis 5.0," ftp://www.aic.nrl.navy.mil/pub/galist/source-code/ga-source (1995).
12. A. Vogel, S. Busch, and U. Parlitz, J. Acoust. Soc. Am. **100**, 148 (1996).
13. G. Heck, J. Ross, and R. J. Levis, Opt. Commun. **259**, 216 (2006).